Journal of King Saud University - Science 36 (2024) 103406

HOSTED BY

Contents lists available at ScienceDirect

Journal of King Saud University - Science

journal homepage: www.sciencedirect.com

Curcumin loaded starch-based aerogels interfere with quorum sensing regulated virulence functions and biofilm of bacterial pathogens

Fohad Mabood Husain [a,*], Mohammed Arshad [b], Rais Ahmad Khan [c], Ahamad Imran [d], Syed Ali Shahzad [a]

[a] Department of Food Science and Nutrition, College of Food and Agriculture Sciences, King Saud University, Riyadh 11451, KSA
[b] Dental Biomaterials Research Chair, College of Applied Medical Science, King Saud University, Riyadh 11451, KSA
[c] Department of Chemistry, College of Science, King Saud University, Riyadh 11451, KSA
[d] King Abdullah Institute of Nanotechnology, College of Science, King Saud University, Riyadh 11451, KSA

ARTICLE INFO

Keywords:
Aerogel
Biofilm
Quorum sensing
Virulence
Antimicrobial resistance

ABSTRACT

Over the last two decades, the sharp escalation of antimicrobial resistance (AMR) has emerged as a formidable threat to human health. This pressing situation demands innovative interventions to combat infectious diseases. Aerogels, characterized by their nanostructured composition and high porosity, present a promising avenue. In this study, we manufactured curcumin loaded starch-based aerogels (CSA) and evaluated their impact on the quorum sensing (QS) mechanism in Gram-negative bacteria. Fourier-transform infrared (FTIR) analysis highlighted the presence of cellulose hydroxyl groups engaged in hydrogen bond formation. Thermogravimetric analysis (TGA) revealed that over 50 % of the initial mass was lost when CSA underwent heating to 350 °C. Microscopic examination showcased a uniform and compact pattern, suggesting reduced pore distribution. The elemental composition analysis indicated that carbon and oxygen constituted 23.00 % and 77.00 % of the weight, respectively. The presence of CSA resulted in over 30.4 % inhibition of violacein pigment production. Furthermore, CSA modulated pyocyanin production, pyoverdin production, LasB elastase activity, and rhamnolipid production by 34.4 %, 31.07 %, 22.7 %, and 19.7 %, respectively. The total exoproteases, cell surface hydrophobicity and exopolysaccharide production in *E. coli*, *L. monocytogenes, S. marcescens*, and *P. aeruginosa*, experienced a significant decrease at sub-MICs. Production of biofilms as well as the mature biofilms in test bacteria were reduced in dose-dependent manner significantly. Due to their antibiofilm and anti-quorum sensing properties, these CSAs could prove to be functional biomaterials with versatile applications, particularly in the food industry.

1. Introduction

Antimicrobial resistance (AMR) poses a substantial risk to human health, as infections caused by multi-drug resistant (MDR) pathogens now stand among the foremost global causes of mortality (Murray et al., 2022). Despite the ground-breaking introduction of antibiotics in the early 20th century, the persistence of pathogens developing resistance due to inappropriate antibiotic usage, encompassing both insufficient and excessive dosing, remains a primary driver for AMR. While the latter part of the 20th century witnessed notable advancements in antibiotic discovery, progress has deaccelerated over the last two decades (Ahmad et al., 2019). The surge in AMR and the lethargic pace of antibiotic discovery have prompted the exploration of inovative interventions. One such strategy involves identifying agents that reduce pathogenicity without hampering bacterial growth, thereby minimizing the likelihood of resistance (Ahmad et al., 2019). Biofilms, pivotal in microbial infections, and quorum sensing emerge as novel targets in drug discovery, with plants showing promise as sources of biofilm and QS inhibitors. QS, a bacterial communication system, entails the density-dependent production of signal molecules that trigger specific gene expression patterns, offering insights into secondary genes governing virulence factors and drug resistance (Rutherford & Bassler, 2012). Notably, the majority of genes expressed during quorum sensing are secondary genes which that are dispensable for the regular bacterial growth and division. These genes encompass factors related to drug resistance, virulence, and various other functionalities.

* Corresponding author.
E-mail address: fhusain@ksu.edu.sa (F. Mabood Husain).

https://doi.org/10.1016/j.jksus.2024.103406
Received 26 May 2024; Received in revised form 20 August 2024; Accepted 20 August 2024
Available online 22 August 2024

Aerogels, first developed by Kistler in 1931, constitute highly porous nanostructured materials with low density, and very large surface area (Kistler, 1931; Nita et al., 2020). Aerogels can be categorized as hybrid inorganic or organic, based on the production material. Organic aerogels, derived from renewable biopolymers like starch, offer a biodegradable alternative to silica aerogels (Nita et al., 2020).

Considering the challenges associated with AMR and the potential of aerogels in combatting them, this research aims to produce and characterize the curcumin loaded starch-based aerogels. The study includes testing the impact of these CSAs on modulating QS of Gram-negative bacteria. Furthermore, a comprehensive analysis was undertaken to assess their effectiveness in inhibiting biofilms of *E. coli*, *S. marcescens*, *L. monocytogenes*, and *P. aeruginosa*.

2. Materials and methods

2.1. Synthesis of curcumin loaded starch-based aerogels

Synthesis of curcumin loaded starch-based aerogels was performed using modified method described previously (García-González & Smirnova, 2013). The starch hydrogels were prepared by dissolving them in double-distilled water (DDW). Gelatinization was attained by heating at 120 ℃ for 20 min at 600 rpm and subsequently cooling it to 85 ℃. These hydrogels were converted to alcogel using solvent exchange process. After the alcogel formation these monoliths were subjected to saturated ethanol solution containing curcumin for two days so that the curcumin penetrates the alcogel internally. Undissolved curcumin was eliminated by centrifugation at 5000 g for 10 min. Curcumin loaded aerogels were fabricated by subjecting the alcogel to supercritical drying.

2.2. Characterization of curcumin loaded starch-based aerogels

Fourier-transform infrared spectroscopy (FTIR) was used to study both intra- and inter-chemical interactions within CSAs, utilizing the Thermo Nicolet 380 spectrometer (Thermo Electron Corporation, USA). The spectral information, obtained in reflectance mode, encompassed a spectrum ranging from 400 to 4000 cm^{-1} at 2 cm^{-1} resolution.

Thermogravimetric analysis (TGA) was conducted to assess thermal characteristics of CSA, employing the TGA Q500 (TA instruments, USA). The aerogel samples were heated to 600 °C from 25 °C with increasing temperature by 5 °C each minute.

DSC was employed to assess the thermal stability of synthesized CSA using the DSC Q2000 differential scanning colorimeter (TA instruments, USA). The aerogel samples were heated to 600 °C from 25 °C with increasing temperature by 5 °C each minute.

The morphology of the surface and the structural network of CSA were scrutinized utilizing the JEOL JSM 6510 LV (Tokyo, Japan) scanning electron microscope (SEM). In this examination, lyophilized CSA (1–2 mg) was affixed to stub and subsequently subjected to gold coating for 5 min. After this process, the curcumin loaded aerogel samples were examined under electron beam to reveal the surface topography. Elemental composition analysis of CSA was carried out using the Oxford INCAx-sight EDAX, integrated with the SEM.

2.3. Growth conditions of bacterial strains used

For this study, *Pseudomonas aeruginosa* PAO1, *Escherichia coli* ATCC 25922, *Listeria monocytogenes* ATCC 19114, and *Serratia marcescens* MTCC 97 were utilized. Each bacterial culture was cultivated in Luria-Bertani (LB) broth under their respective growth conditions.

2.4. Examination of minimum inhibitory concentration (MIC)

The determination of MIC of CSA against all test pathogens involved the utilization of TTC dye, following a well-established method described previously (Qais et al., 2018).

2.5. Examination of violacein production

The extraction and quantitative assessment of violacein followed a previously delineated methodology (Matz et al., 2004). Briefly, *C. violaceum* 12,472 cultured overnight in the presence and absence of CSA were subjected to centrifugation. The resulting pellet was reconstituted in DMSO (1 ml), and then vortexed vigorously to solubilize the pigment. Absorbance was taken at 585 nm.

2.6. Examination of prodigiosin production

To assess the production of prodigiosin, *S. marcescens* cells were subjected to a 24-hour cultivation, both with and without the presence of CSA. Post-cultivation, cells were harvested through centrifugation and prodigiosin was extracted from collected cells. This quantification was done by taking the absorbance at 534 nm, as detailed earlier (Slater et al., 2008).

2.7. Examination of virulent traits in P. Aeruginosa

The assessment for pyocyanin was performed meticulously using the Pseudomonas broth (PB) medium. PAO1 underwent cultivation both without and with CSA, over 18 h. Pyocyanin concentration expressed in μg/ml, was then determined utilizing a calculation elucidated previously (Husain et al., 2017).

The pyoverdin assay adhered to a previously delineated method (Ankenbauer et al., 1985). Briefly, an overnight grown PAO1 culture (without and with CSA) was subjected to centrifugation. Next, 100 ÂμI of supernatant were mixed with 900 μl Tris-HCl buffer (50 mM, pH 7.4). The fluorescence of resulting sample was measured at 460 nm, with excitation at 400 nm.

The assessment of elastolytic activity involved the use of elastin congo red (ECR), as described previously (Kessler et al., 1982). Specifically, 100 μl cell free supernatant cultured with and without CSA was added to 900 μl ECR buffer. To impede the reaction, 1 ml sodium phosphate buffer was added, insoluble ECR was separated, and absorbance of resulting solution was read at 495 nm.

The rhamnolipid assay was conducted using the orcinol method, making minor adjustments based on a previously established protocol (Husain et al., 2017). Specifically, 0.3 ml supernatant from both CSA-treated and untreated cultures was extracted diethyl ether. Following separation, organic solvent was evaporated and reconstituted in deionized water (100 μl). Orcinol solution (900 μl) was added to each sample and heated at 80 °C for half hour. After cooling, the mixture was read at 421 nm.

2.8. Examination of total exoproteases

The assessment of exoprotease activity in all test bacteria involved the implementation of azocasein-degradation assay (Husain et al., 2017). Concisely, 100 μl cell-free supernatant was mixed with 0.3 % azocasein and then incubated for 15 min at 37 °C. TCA (500 μl) was introduced, followed by centrifugation. Absorbance was measured at 400 nm.

2.9. Assessment of cell surface hydrophobicity (CSH)

CSH was evaluated employing xylene, following a previously detailed procedure (Rosenberg et al., 1980). Concisely, 1 ml of overnight-grown culture and 0.1 ml of xylene was mixed along with sub-MICs of CSA. The resulting mixture was vortexed and incubated for 10 min. Absorbance of aqueous phase was later recorded at 530 nm. The % hydrophobicity was determined by applying the formula:

$$\%hydrophobicity = \left[1 - \frac{ODaftervortexing}{ODbeforevortexing}\right] \times 10 \quad (1)$$

2.10. Measurement of the exopolysaccharides secreted by bacteria

The quantification of exopolysaccharides (EPS) levels in cultures, both untreated and treated with CSA, was performed following a standard procedure with slight modifications (Hasan et al., 2019). This process facilitated the precipitation of EPS. To quantify the EPS, the Dubois method was used (DuBois et al., 1956).

2.11. Inhibition of biofilm formation

Biofilm inhibition experiments were systematically conducted utilizing a 96-well microtiter plate (MTP) (Husain et al., 2017). Briefly, overnight cultures of test pathogens were introduced into wells of MTP with 0.15 ml LB medium. Various concentrations of CSA were administered as the treatment groups, while untreated control groups, were also incorporated. MTP was incubated for 24-hour. Subsequently, cells were washed thrice with phosphate buffer. Developed biofilms underwent staining for 20 min in 0.2 ml crystal violet, followed by a gentle wash. The conjugated dye was then dissolved in ethanol, and optical density was taken at 620 nm.

2.12. Disruption of preformed biofilms

The biofilm disruption assay was conducted following a standard procedure with slight modifications. All test bacteria were cultivated in microtiter plates for a 24-hour period, allowing the formation of biofilms within the plate wells. Following this, the protocol described above was used to assess the effect of CSA on preformed biofilms.

2.13. Statistical analysis

Students *t*-test was used to determine the significance ($p \leq 0.05$) between control and treatment. Data are presented as mean of triplicates.

3. Results and discussion

In the present study, curcumin loaded starch-based aerogels were synthesized using supercrirtical-CO_2 drying, stored at room temperature and were characterized using various microscopic and spectroscopic techniques.

3.1. Fourier-transform infrared spectroscopy

The cross-linking of cellulose is essential for maintaining its integrity and structural stability. Analysing the physicochemical changes in CSA is vital, as any alterations in structure can impact their biological properties. FTIR analysis was conducted to validate intermolecular interactions, as depicted in Fig. 1, showcasing CSA's FTIR spectrum. The IR spectrum revealed distinctive absorption peaks characteristic of the polymer. Notably,

The absorption peak in from 3000 to 3600 cm^{-1} is due to the stretching vibrations of hydroxyl group participating in hydrogen bond formation. (Revin et al., 2020). Two minor peaks around 1640 and 1680 cm^{-1} are attributed to deformation vibrations of hydroxyl group from adsorbed water. One intense band at 1410 cm^{-1} is an indicator of CH_2 bending vibrations (Cael et al., 1975). Furthermore, a prominent peak at 1020 cm^{-1} aligns with valence vibrations of C–O bonds (Revin et al., 2020). In summary, the FTIR spectra provided insights into the chemical bonds and vibrations present in cellulose-loaded curcumin nanoparticles.

3.2. Thermogravimetric analysis

The temperature stability of CSA is a critical trait, mainly in high-

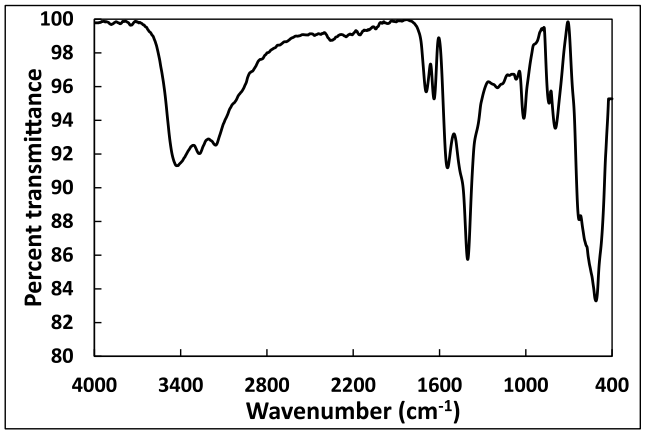

Fig. 1. Fourier-transform infrared spectroscopy (FTIR) spectra of curcumin aerogels from 4000 to 400 cm-1.

thermal functions of this material. To assess this, a TGA was conducted on CSA, and the thermal decomposition along with the first derivative is illustrated in Fig. 2**A**. The weight loss of CSA started at early temperatures and around 150 °C, more than 20 % mass loss was observed. This initial loss is attributed to water evaporation present in CSA (Huang et al., 2014). TGA further indicated that at 350 °C, more than 50 % of the initial mass was lost. Upon reaching 500 °C, a substantial 62.05 % loss of the initial mass of CSA was recorded. This finding aligns with the thermogravimetric characteristics of the thermal stability of CSA (Rostamitabar et al., 2022).

3.3. DSC

To verify the degradation of the synthesized aerogel material with respect to heat flow, DSC analysis was done until 400℃. The findings are given in Fig. 2**B** where material shows two endothermic peaks and one exothermic peak. The first endothermic peak appearing at 60.45 ℃ is due to removal of adsorbed humidity from nanoparticle surface. The other endothermic peak that appeared at 131.95 ℃ is due to the melting or fusion of the material. At this stage, the polysaccharide undergoes 1,4-linked bond breakage, and pyranose chair distortion under temperature variation. The exothermic peak appearing at 250.63 ℃ is due to the crystallization process of the fused material. The DSC curve of the aerogel supports the TGA data.

3.4. Scanning electron microscopy (SEM)

The surface topography of CSA underwent examination through SEM. Fig. 3**A–B** showcasing SEM images at both 25000X and 10000X magnifications, respectively. These images reveal CSA with smooth surfaces and distinctive three-dimensional structures (Dharunya et al., 2016). At higher magnifications, grooves can also be seen, suggesting reduced pore distribution possibly attributed to heightened cross-linking. This intensified cross-linking enhances both intra- and intermolecular interactions, fostering the development of well-interconnected three-dimensional CSA (Dharunya et al., 2016). Importantly, aerogel surface characteristics play a pivotal role in regulating cell attachment. The grooved porous matrices can effectively serve as scaffolds, accommodating numerous cells on their grooved surfaces. These findings are consistent with a previous report, highlighting the potential of CSA as biocompatible matrices (Revin et al., 2020). Additionally, EDX analysis for elemental composition, depicted in Fig. 3**C**, reveals a weight percentage of 23.00 % for carbon and 77.00 % for oxygen. In terms of atomic percentage, carbon and oxygen are represented at 28.46 % and 71.53 %, respectively. The uniform distribution of carbon and oxygen visualized using the elemental mapping analysis

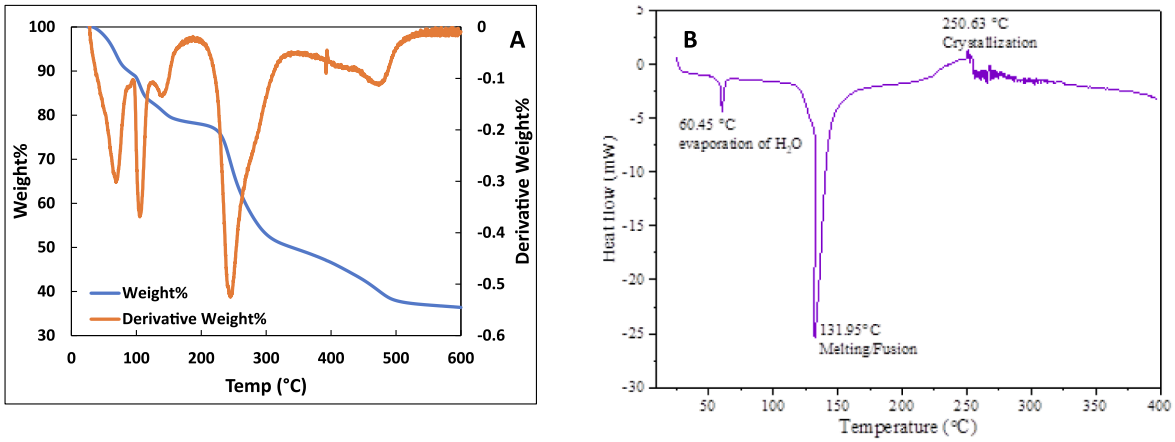

Fig. 2. A. Thermogravimetric analysis (TGA) graphs of the curcumin aerogels. The initial weight loss till 100 °C came from the vaporization of water and the second step at 200–300 °C was the relatively rapid decomposition. Secondary y-axis shows derivative thermogravimetry of cellulose aerogels from 25 °C to 600 °C. 2B. DSC curve of the CSA.

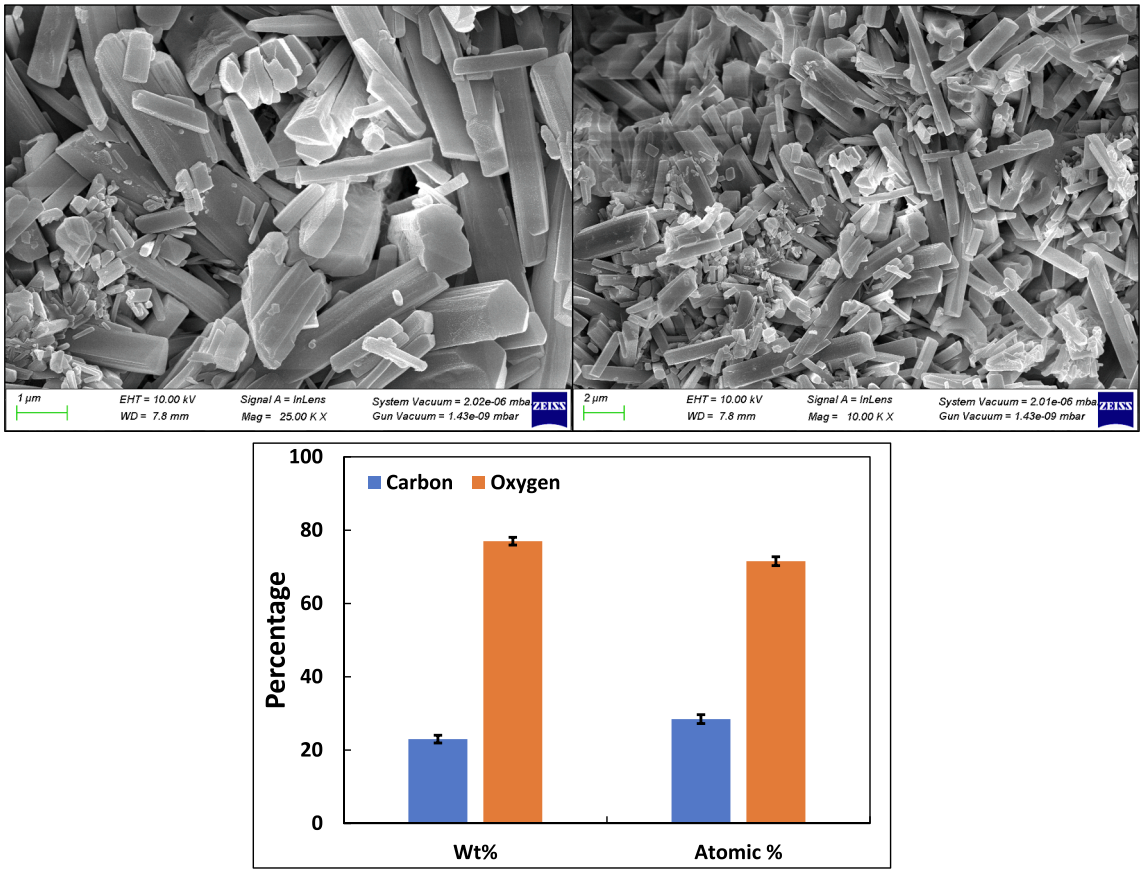

Fig. 3. (A) SEM image of curcumin aerogels at 25000X magnification. (B) SEM image of cellulose aerogels at 10000X magnification. (C) Elemental analysis of curcumin aerogels.

demonstrates the effective synthesis methodology applied (Fig. 4).

3.5. Determination of MIC

MIC of the synthesized aerogels against all test pathogens was recorded as 8 mg/ml. All assays were conducted at sub-MICs i.e. below the MIC.

3.6. CSA inhibition the violacein production

The spectrophotometric analysis was aimed at quantifying violacein inhibition. Violacein production in *C. violaceum* 12,472 decreased as the concentrations of CSA increased (Fig. 5). When exposed to 1 mg/ml and 2 mg/ml CSA, there were reductions in pigment production, corresponding to 5.4 %, and 17.7 %, respectively. The highest sub-MIC concentration tested (4 mg/ml) demonstrated a significant 30.4 % inhibition of violacein. These outcomes robustly affirm the pronounced

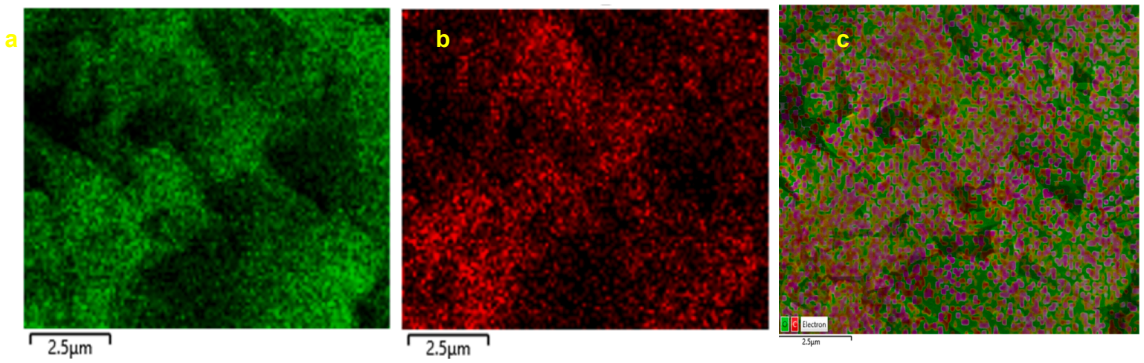

Fig. 4. Elemental of curcumin loaded starch based aerogels (a) oxygen. (b) carbon. (c) mixed mapping of oxygen and carbon.

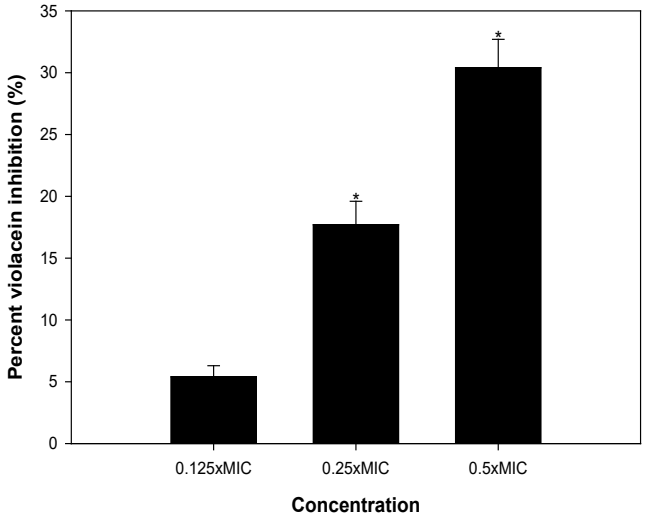

Fig. 5. Effect of sub-MICs of CSA on violacein production in *C. violaceum.*

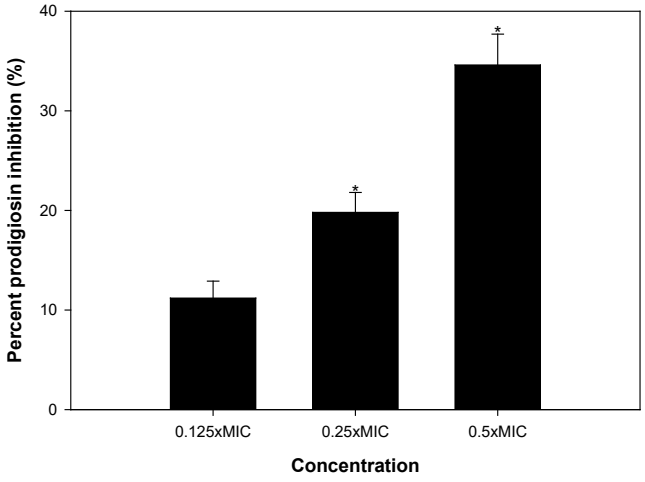

Fig. 6. Effect of sub-MICs of CSA on prodigiosin production in *S. marcescens.*

inhibitory influence of CSA on quorum sensing-regulated production of violacein in *C. violaceum* 12472. In *C. violaceum*, the production of violacein is controlled by CviIR quorum sensing system and the observed pigment reduction is indicative of anti-QS potential of CSA.

3.7. CSA inhibits the prodigiosin

Prodigiosin is a distinctive red pigment in *S. marcescens*, with its synthesis intricately governed by quorum sensing mechanisms (Morohoshi et al., 2007). The data illustrated in Fig. 6 unveils a dose-dependent suppression of prodigiosin induced by CSA. The inhibition percentages for this pigment were measured at 11.2 %, 19.8 % and 34.6 % when treated with concentrations of 1, 2, and 4 mg/ml of CSA, respectively. It's noteworthy that certain strains of *S. marcescens* reveal shared regulatory mechanisms connecting prodigiosin biogenesis to other phenotypes such as flagellar variation, hemagglutination, and protease production (Goluszko et al., 1995). These findings underscore the potential of CSA in modulating prodigiosin synthesis in *S. marcescens*, offering insights into their quorum sensing regulatory effects.

3.8. Inhibition of virulent traits of P. Aeruginosa PAO1 by CSA

Pyoverdin is a fluorescent siderophore that is secreted by *P. aeruginosa,* contributing in the virulence and host infection (Peek et al., 2012). CSA at 2 and 4 mg/ml inhibited the pyoverdin secretion by 17.1 % and 31 %, respectively, with respect to control (Fig. 7). Pyoverdin helps *P. aeruginosa* to cause disease by binding to transferrin

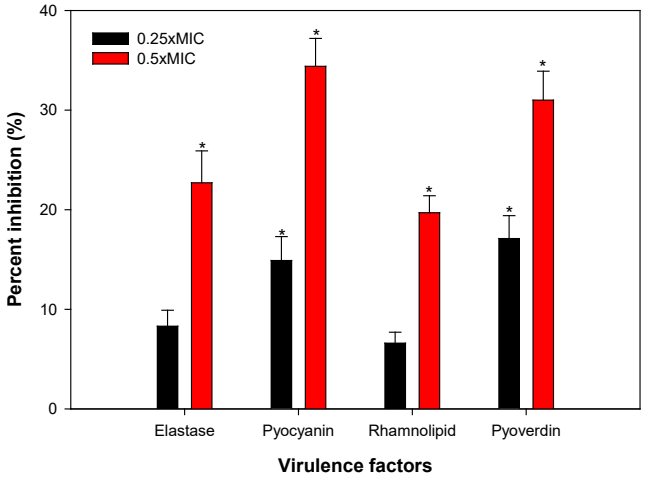

Fig. 7. Effect of sub-MICs of CSA on QS regulated virulence factor production in *P. aeruginosa* PAO1.

protein, causing deficiency of iron in mammalian host tissues, escapes detection by lipocalin (linked to neutrophil gelatinase), which helps *P. aeruginosa* to infect, especially in lungs of patents with cystic fibrosis (Das et al., 2016; Peek et al., 2012). Thus, we expect that any chemotherapeutic agent that lowers pyoverdin production would reduce the pathogenicity of these bacteria. The observed reduction in pyoverdin secretion by CSA suggests a potential mechanism of combatting

P. aeruginosa virulence and may hinder the pathogen's ability to establish infection. This has important implications for developing strategies to combat *P. aeruginosa* infections, particularly in contexts such as cystic fibrosis.

Pyocyanin, a blue-green pigment, acts as a virulence factor for *P. aeruginosa*. It is acknowledged for its role in *P. aeruginosa* pathogenicity, as it hinders with many cellular functions. The severity of the disease is also linked to the oxidative stress caused by pyocyanin (Hunter et al., 2012). Moreover, it suppresses the host's defense system, leading to an increased rate of apoptosis in human neutrophils, and it also supports in biofilm development (Das et al., 2015). Decreased pyocyanin production was recorded upon treatment with CSA, as detailed in Fig. 7. Concentrations of 2 and 4 mg/ml of CSA resulted in reduced pyocyanin production by 14.9 % and 34.4 %, respectively. The observed inhibitory effect of CSA on pyocyanin production suggests a potential strategy for mitigating *P. aeruginosa* virulence. By reducing the pyocyanin levels, CSA may contribute to the attenuation of *P. aeruginosa* pathogenicity.

The examination of CSA's potential to diminish elastase activity was undertaken. The results, presented in Fig. 7, displayed a discernible effect in *P. aeruginosa* PAO1 supernatant, on comparing with untreated control. Specifically, at 4 mg/ml of CSA, there was a noteworthy 22.7 % decrease in LasB elastase activity. *P. aeruginosa* is known for producing an array of hydrolytic enzymes, including elastases, that are implicated in tissue degradation and interference with host immune mechanisms (Bandara et al., 2006). Reduction in elastolytic enzyme activity indicates CSA also targets LasI-LasR system of *P. aeruginosa*. The downregulation of LasB elastase activity indicates a potential disruption of QS system, influencing biofilm development and virulence factors.

Likewise, the application of CSA exhibited a suppressive effect on rhamnolipid production in *P. aeruginosa* PAO1 (Fig. 7**)**. At tested sub-MICs of 2 and 4 mg/ml CSA, reduction in rhamnolipid production was observed, amounting to 5.6 %, and 19.7 %, respectively. Rhamnolipids, known for their involvement in quorum sensing-mediated motility (mainly swimming) and dispersal of biofilm at infection sites, play a crucial role in *P. aeruginosa*'s pathogenicity (O'May & Tufenkji, 2011). The observed reduction in rhamnolipid production in response to CSA highlights their potential to modulate key quorum sensing-mediated processes in *P. aeruginosa*. The inhibitory effect on rhamnolipid production suggests a potential strategy for disrupting bacterial virulence and reducing biofilm-related infections.

3.9. Effect of CSA on total exoproteases, cell surface hydrophobicity (CSH) and EPS

Protease assay was utilized to measure the total exoproteases in the culture supernatant treated with CSA. CSA at 4 mg/ml reduced the azocasein-degrading protease levels in *P. aeruginosa* PAO1 by 29.7 %, compared to untreated control (Fig. 8). Likewise, the total proteases in *S. marcescens*, *L. monocytogenes*, and *E. coli* decreased by 32 %, 19.1 %, and 28.6 %, respectively when treated with 4 mg/ml of CSA. The highest inhibition of 37.2 % in total exoproteases was observed for *C. violaceum*. Proteases can enhance invasion by bacteria by degrading the proteins of host cells and evading the host defense system. These results show the potential of CSA to regulate exoprotease production in different bacterial strains, which may have implications for bacterial pathogenesis and host interactions.

The effect of CSA on the CSH was evaluated, which is important for the attachment and biofilm formation in pathogenic bacteria on solid surfaces. When exposed to 4 mg/ml of CSA, the CSH was reduced to 21.8 %, 20.4 %, 32.3 %, 21.5 % and 26.3 % in *P. aeruginosa*, *S. marcescens*, *L. monocytogenes*, *E. coli* and *C. violaceum* respectively, as shown in Fig. 8. These results indicate the potential of CSA to modulate bacterial surface characteristics, affecting their ability to adhere and establish biofilms, which has implications for bacterial pathogenesis and biofilm-related infections.

Exopolysaccharide (EPS) production is vital for biofilms as it

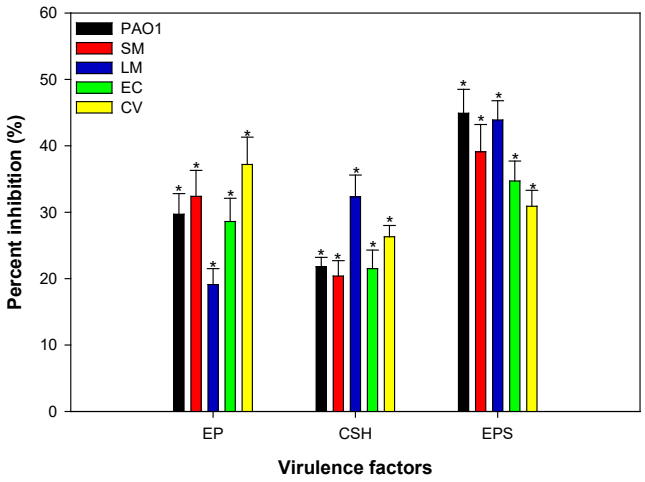

Fig. 8. Effect of sub-MICs of CSA on virulence factor production in test pathogens.

maintains its architecture and shields the biofilm from being disrupted by antimicrobials (Flemming and Wingender, 2010). At the highest tested sub-MIC (4 mg/ml) of CSA, reduced EPS production was observed in all the test pathogens (Fig. 8**)**. EPS production was impaired by 44.9 %, 39.1 %, 43.9 %, 34.7 %, and 30.9 % in *P. aeruginosa*, *S. marcescens*, *L. monocytogenes*, *E. coli* and *C. violaceum*, respectively. TiO_2 nanoparticles, synthesized from *W. somnifera* aqueous extract, is documented for their efficacy in inhibiting EPS production in various bacterial strains including *E. coli, L. monocytogenes, P. aeruginosa*, MRSA, and *S. marcescens*, (Al-Shabib et al., 2020). The decreased EPS production will adversely affect the viability of the biofilm. It is envisaged that the biofilms will become weak and more susceptible to antimicrobials and easier to be taken over by host's immune system.

3.10. CSA inhibits the biofilm development

The *P. aeruginosa* pathogenicity is also linked to the formidable biofilms that confer enhanced resistance to both chemical and physical treatments. The process of biofilm development is highly organized, intricate, and tightly regulated, often intricately linked with bacterial cellular communication, particularly QS mechanisms (Qin et al., 2015). It is noteworthy that nearly 80 % human infections are facilitated by the presence of biofilms. The persistence of biofilms is intricately associated with matrix, mainly composed of exopolysaccharides (EPS) (Flemming & Wingender, 2010). Biofilms are formed by bacteria on various substrates, leading to associated infections in humans, plants, and animals (Kannappan et al., 2020).

As illustrated in Fig. 9, the CSA demonstrated a significant reduction in biofilm formation. Specifically, treatment with 4 mg/ml concentrations of CSA led to diminished biofilm formation in *P. aeruginosa*, *L. monocytogenes*, *S. marcescens*, *E. coli* and *C. violaceum* by 40.5 %, 44.6 %, 47.2 %, 51.2 % and 41.8 %, respectively, with respect to control. This evidence underscores the potential of CSA, modulating biofilm formation across various bacterial strains.

3.11. CSA disrupts the established biofilms

Majority of antibiotics mainly target planktonic cells of bacterial, and only a limited number of antibiotics are known to effectively inhibit the development of biofilms (Roy et al., 2018). Inhibiting biofilms during their formation is easier compared to eradicating preformed biofilms. The impact of CSA on the disruption of established biofilms is illustrated in Fig. 10. The presence of 4 mg/ml of CSA resulted in the removal of formed biofilms of *P. aeruginosa* PAO1 by 38.1 %. Similarly,

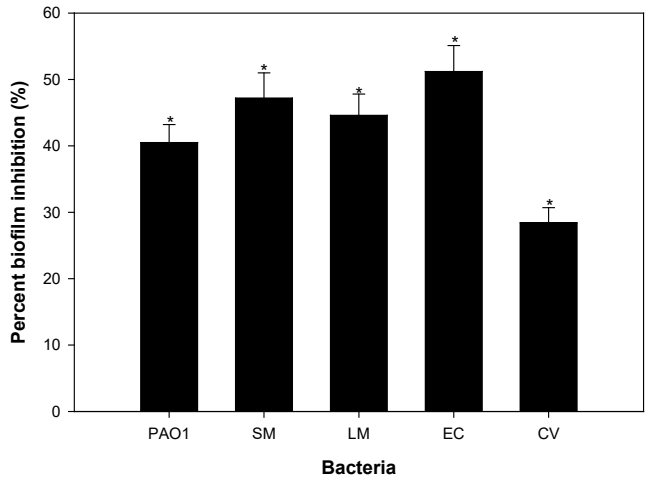

Fig. 9. Effect of sub-MICs of CSA on biofilm formation in test pathogens.

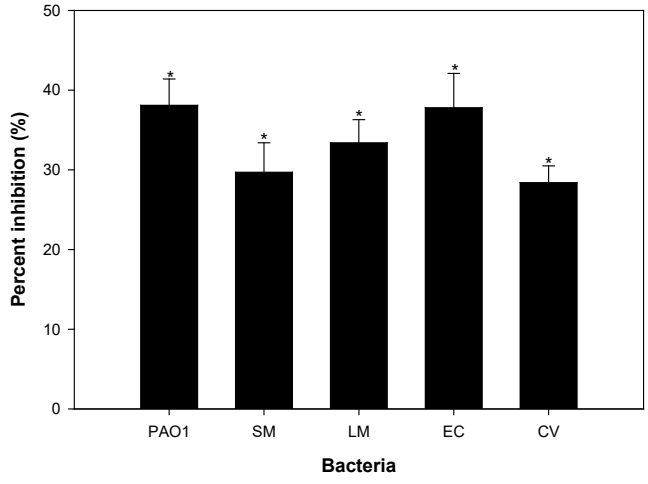

Fig. 10. Effect of sub-MICs of CSA on pre-formed (mature) biofilms in test pathogens.

preformed biofilms of *L. monocytogenes*, *S. marcescens*, *E. coli* and *C. violaceum* were reduced by 33.4 %, 29.7 %, 37.8 %, and 28.4 % in presence of 4 mg/ml CSA. The data presented illustrate the effective eradication of biofilms formed by the bacteria. The findings align with our prior report where preformed biofilms of *P. aeruginosa*, *E. coli*, MRSA, and *L. monocytogenes* were successfully disrupted (Al-Shabib et al., 2020). The results unequivocally indicate that CSA exhibited efficacy both in eradicating and inhibiting the biofilms formed by of test bacteria. This dual action underscores the potential of CSA as a versatile strategy for addressing biofilm-associated infections, offering promise in both prevention and intervention approaches against bacterial biofilm formation.

4. Conclusion

Taken together, our findings highlight the efficacy of curcumin loaded starch aerogels in interfering with bacterial quorum sensing and mitigating the formation of biofilm as well as reducing mature biofilms in foodborne pathogens. These results of this study could lead to the development of novel antibiofilm agents. Furthermore, these aerogels can be utilized for the development of a paradigm that limits the biofilm formation not only in food industry but can prove effective clinically also.

CRediT authorship contribution statement

Fohad Mabood Husain: Writing – review & editing, Writing – original draft, Project administration, Investigation, Funding acquisition, Formal analysis, Data curation, Conceptualization. **Mohammed Arshad:** Writing – review & editing, Validation, Investigation, Formal analysis, Data curation. **Rais Ahmad Khan:** . **Ahamad Imran:** Writing – review & editing, Validation, Software, Resources. **Syed Ali Shahzad:** Validation, Software, Resources, Investigation.

Declaration of Competing Interest

The authors declare that they have no known competing financial interests or personal relationships that could have appeared to influence the work reported in this paper.

Acknowledgement

The authors extend their appreciation to the Deputyship for Research & Innovation, "Ministry of Education" in Saudi Arabia for funding this research work through the project number (IFKSUDR_F104).

References

Ahmad, I., Qais, F., Samreen, Abulreesh, H., Ahmad, S., & Rumbaugh, K. (2019). Antibacterial Drug Discovery: Perspective Insights. In *Antibacterial Drug Discovery to Combat MDR* (pp. 1–21). Springer Singapore. DOI: 10.1007/978-981-13-9871-1_1.

Al-Shabib, N.A., Husain, F.M., Qais, F.A., Ahmad, N., Khan, A., Alyousef, A.A., Arshad, M., Noor, S., Khan, J.M., Alam, P., Albalawi, T.H., Shahzad, S.A., 2020. Phyto-Mediated Synthesis of Porous Titanium Dioxide Nanoparticles from Withania somnifera Root Extract: Broad-Spectrum Attenuation of Biofilm and Cytotoxic Properties Against HepG2 Cell Lines. Front. Microbiol. 11 https://doi.org/10.3389/fmicb.2020.01680.

Ankenbauer, R., Sriyosachati, S., Cox, C.D., 1985. Effects of siderophores on the growth of Pseudomonas aeruginosa in human serum and transferrin. Infect. Immun. 49 (1), 132–140.

Bandara, M.B.K., Zhu, H., Sankaridurg, P.R., Willcox, M.D.P., 2006. Salicylic Acid Reduces the Production of Several Potential Virulence Factors of Pseudomonas aeruginosa Associated with Microbial Keratitis. Investigative Opthalmology & Visual Science 47 (10), 4453. https://doi.org/10.1167/iovs.06-0288.

Cael, J.J., Gardner, K.H., Koenig, J.L., Blackwell, J., 1975. Infrared and Raman spectroscopy of carbohydrates. Paper V. Normal coordinate analysis of cellulose I. J. Chem. Phys. 62 (3), 1145–1153. https://doi.org/10.1063/1.430558.

Das, T., Kutty, S.K., Tavallaie, R., Ibugo, A.I., Panchompoo, J., Sehar, S., Aldous, L., Yeung, A.W.S., Thomas, S.R., Kumar, N., Gooding, J.J., Manefield, M., 2015. Phenazine virulence factor binding to extracellular DNA is important for Pseudomonas aeruginosa biofilm formation. Sci. Rep. 5 https://doi.org/10.1038/srep08398.

Das, M.C., Sandhu, P., Gupta, P., Rudrapaul, P., De, U.C., Tribedi, P., Akhter, Y., Bhattacharjee, S., 2016. Attenuation of Pseudomonas aeruginosa biofilm formation by Vitexin: A combinatorial study with azithromycin and gentamicin. Sci. Rep. 6 (1), 23347. https://doi.org/10.1038/srep23347.

de la Fuente-Núñez, C., Reffuveille, F., Fernández, L., Hancock, R.E., 2013. Bacterial biofilm development as a multicellular adaptation: antibiotic resistance and new therapeutic strategies. Curr. Opin. Microbiol. 16 (5), 580–589. https://doi.org/10.1016/j.mib.2013.06.013.

Dharunya, G., Duraipandy, N., Lakra, R., Korapatti, P.S., Jayavel, R., Kiran, M.S., 2016. Curcumin cross-linked collagen aerogels with controlled anti-proteolytic and pro-angiogenic efficacy. Biomed. Mater. 11 (4), 045011 https://doi.org/10.1088/1748-6041/11/4/045011.

DuBois, M., Gilles, K.A., Hamilton, J.K., Rebers, P.A., Smith, F., 1956. Colorimetric Method for Determination of Sugars and Related Substances. Anal. Chem. 28 (3), 350–356. https://doi.org/10.1021/ac60111a017.

Flemming, H.-C., Wingender, J., 2010. The biofilm matrix. Nat. Rev. Microbiol. 8 (9), 623–633. https://doi.org/10.1038/nrmicro2415.

Goluszko, P., Nowicki, B., Goluszko, E., Nowicki, S., Kaul, A., Pham, T., 1995. Association of colony variation in Serratia marcescens with the differential expression of protease and type 1 fimbriae. FEMS Microbiol. Lett. 133 (1–2), 41–45.

Gupta, P., Singh, B., Agrawal, A.K., Maji, P.K., 2018. Low density and high strength nanofibrillated cellulose aerogel for thermal insulation application. Mater. Des. 158, 224–236. https://doi.org/10.1016/j.matdes.2018.08.031.

Hasan, I., Qais, F.A., Husain, F.M., Khan, R.A., Alsalme, A., Alenazi, B., Usman, M., Jaafar, M.H., Ahmad, I., 2019. Eco-friendly green synthesis of dextrin based poly (methyl methacrylate) grafted silver nanocomposites and their antibacterial and antibiofilm efficacy against multi-drug resistance pathogens. J. Clean. Prod. 230, 1148–1155. https://doi.org/10.1016/j.jclepro.2019.05.157.

Hunter, R.C., Klepac-Ceraj, V., Lorenzi, M.M., Grotzinger, H., Martin, T.R., Newman, D. K., 2012. Phenazine Content in the Cystic Fibrosis Respiratory Tract Negatively

Correlates with Lung Function and Microbial Complexity. Am. J. Respir. Cell Mol. Biol. 47 (6), 738–745. https://doi.org/10.1165/rcmb.2012-0088OC.

Husain, F.M., Ahmad, I., Al-Thubiani, A.S., Abulreesh, H.H., AlHazza, I.M., Aqil, F., 2017. Leaf extracts of Mangifera indica L. inhibit quorum sensing - Regulated production of virulence factors and biofilm in test bacteria. Front. Microbiol. 8 (APR), 727. https://doi.org/10.3389/fmicb.2017.00727.

Kannappan, A., Durgadevi, R., Srinivasan, R., Lagoa, R.J.L., Packiavathy, I.A.S.V., Pandian, S.K., Veera Ravi, A., 2020. 2-Hydroxy-4-methoxybenzaldehyde from Hemidesmus indicus is antagonistic to Staphylococcus epidermidis biofilm formation. Biofouling 36 (5), 549–563. https://doi.org/10.1080/08927014.2020.1777989.

Kessler, E., Israel, M., Landshman, N., Chechick, A., Blumberg, S., 1982. In vitro inhibition of Pseudomonas aeruginosa elastase by metal-chelating peptide derivatives. Infect. Immun. 38 (2), 716–723.

Kistler, S.S., 1931. Coherent Expanded Aerogels and Jellies. Nature 127 (3211), 741. https://doi.org/10.1038/127741a0.

Matz, C., Deines, P., Boenigk, J., Arndt, H., Eberl, L., Kjelleberg, S., Jurgens, K., 2004. Impact of Violacein-Producing Bacteria on Survival and Feeding of Bacterivorous Nanoflagellates. Appl. Environ. Microbiol. 70 (3), 1593–1599. https://doi.org/10.1128/AEM.70.3.1593-1599.2004.

Morohoshi, T., Shiono, T., Takidouchi, K., Kato, M., Kato, N., Kato, J., Ikeda, T., 2007. Inhibition of Quorum Sensing in Serratia marcescens AS-1 by Synthetic Analogs of N-Acylhomoserine Lactone. Appl. Environ. Microbiol. 73 (20), 6339–6344. https://doi.org/10.1128/AEM.00593-07.

Murray, C. J. L., Ikuta, K. S., Sharara, F., Swetschinski, L., Robles Aguilar, G., Gray, A., Han, C., Bisignano, C., Rao, P., Wool, E., Johnson, S. C., Browne, A. J., Chipeta, M. G., Fell, F., Nita, L. E., Ghilan, A., Rusu, A. G., Neamtu, I., & Chiriac, A. P. (2020). New Trends in Bio-Based Aerogels. *Pharmaceutics*, *12*(5), 449. DOI: 10.3390/pharmaceutics12050449.

O'May, C., Tufenkji, N., 2011. The Swarming Motility of Pseudomonas aeruginosa Is Blocked by Cranberry Proanthocyanidins and Other Tannin-Containing Materials. Appl. Environ. Microbiol. 77 (9), 3061–3067. https://doi.org/10.1128/AEM.02677-10.

Peek, M.E., Bhatnagar, A., McCarty, N.A., Zughaier, S.M., 2012. Pyoverdine, the Major Siderophore in Pseudomonas aeruginosa, Evades NGAL Recognition. Interdisciplinary Perspectives on Infectious Diseases 2012. https://doi.org/10.1155/2012/843509.

Revin, V.V., Nazarova, N.B., Tsareva, E.E., Liyaskina, E.V., Revin, V.D., Pestov, N.A., 2020. Production of Bacterial Cellulose Aerogels With Improved Physico-Mechanical Properties and Antibacterial Effect. Front. Bioeng. Biotechnol. 8 https://doi.org/10.3389/fbioe.2020.603407.

Rosenberg, M., Gutnick, D., Rosenberg, E., 1980. Adherence of bacteria to hydrocarbons: A simple method for measuring cell-surface hydrophobicity. FEMS Microbiol. Lett. 9 (1), 29–33. https://doi.org/10.1111/j.1574-6968.1980.tb05599.x.

Rostamitabar, M., Ghahramani, A., Seide, G., Jockenhoevel, S., Ghazanfari, S., 2022. Drug loaded cellulose–chitosan aerogel microfibers for wound dressing applications. Cellul. 29 (11), 6261–6281. https://doi.org/10.1007/s10570-022-04630-6.

Roy, R., Tiwari, M., Donelli, G., Tiwari, V., 2018. Strategies for combating bacterial biofilms: A focus on anti-biofilm agents and their mechanisms of action. Virulence 9 (1), 522–554. https://doi.org/10.1080/21505594.2017.1313372.

Rutherford, S.T., Bassler, B.L., 2012. Bacterial Quorum Sensing: Its Role in Virulence and Possibilities for Its Control. Cold Spring Harb. Perspect. Med. 2 (11), a012427. https://doi.org/10.1101/cshperspect.a012427.